# Orbital Decomposition of the Carbon Chemical Shielding Tensor in Gold(I) N-Heterocyclic Carbene Complexes

Izquierdo, Maria A.; Tarantelli, Francesco; Broer, Ria; Bistoni, Giovanni; Belpassi, Leonardo; Havenith, Remco W. A.

*Published in:*
European Journal of Inorganic Chemistry

*DOI:*
10.1002/ejic.201901115



*Publication date:*
2020

EurJIC
European Journal of Inorganic Chemistry

Full Paper
doi.org/10.1002/ejic.201901115

Gold(I) NHC Complexes

# Orbital Decomposition of the Carbon Chemical Shielding Tensor in Gold(I) N-Heterocyclic Carbene Complexes

Maria A. Izquierdo,*[a,b] Francesco Tarantelli,[c,d] Ria Broer,[a] Giovanni Bistoni,[e] Leonardo Belpassi,[d] and Remco W. A. Havenith*[a,f,g]

**Abstract:** The good performance of N-heterocyclic carbenes (NHCs), in terms of versatility and selectivity, has called the attention of experimentalists and theoreticians attempting to understand their electronic properties. Analyses of the Au(I)–C bond in $[(NHC)AuL]^{+/0}$ (L stands for a neutral or negatively charged ligand), through the Dewar–Chatt–Duncanson model and the charge displacement function, have revealed that NHC is not purely a $\sigma$-donor but may have a significant $\pi$-acceptor character. It turns out, however, that only the $\sigma$-donation bonding component strongly correlates with one specific component of the chemical shielding tensor. Here, in extension to earlier works, a current density analysis, based on the continuous transformation of the current density diamagnetic zero approach, along a series of $[(NHC)AuL]^{+/0}$ complexes is presented. The shielding tensor is decomposed into orbital contributions using symmetry considerations together with a spectral analysis in terms of occupied to virtual orbital transitions. Analysis of the orbital transitions shows that the induced current density is largely influenced by rotational transitions. The orbital decomposition of the shielding tensor leads to a deeper understanding of the ligand effect on the magnetic response properties and the electronic structure of (NHC)-Au fragments. Such an orbital decomposition scheme may be extended to other magnetic properties and/or substrate-metal complexes.

## Introduction

N-heterocyclic carbenes (NHCs) have emerged as substrates for transition metal catalysts due to their electron-donating features.[1,2] NHCs have, unlike traditional carbenes, a neutral divalent carbon stabilized by electron donation from one or more adjacent nitrogen atoms into the empty carbon 2p orbital. When NHCs are coordinated to a metal center, NHCs behave as strong $\sigma$-donor ligands, even stronger than alkyl phosphines, which in many cases lead to a greater stability of the pre-catalysts or catalysts.[3] The NHC-metal bond stability has made NHCs quite attractive, not only for experimentalists in regard to the ligand design, but also for theoreticians who attempt to understand their electronic properties.[4–7] The nature of the NHC-Au bond in $[(NHC)AuL]^{+/0}$ complexes strongly depends on the electronic structure of L and NHC. NHC is not a pure $\sigma$-donor but may have $\pi$-acceptor character, being entirely negligible {as found in $[(NHC)AuCO]^+$} or accounting up to half of the $\sigma$-donor character {as found in [(NHC)AuCl]}.[8] A more comprehensive overview of the chemistry of N-heterocyclic carbenes is given in ref.,[9] and recently [(NHC)AgX] compounds were synthesized.[10] The bonding properties of the carbene–Au bond (also Ag/Cu were considered) in [(NHC)AuCl] and metal-biscarbenes have been investigated using an energy decomposition analysis. It was found that the carbene–Au bond has a large electrostatic component, and the orbital part consists of approximately 20 % $\pi$ backbonding.[11] A further extensive computational study[12] showed that also higher coordination numbers are within reach, and that the $\pi^*$-back-donation can serve as a design criterion.

A charge displacement study of different [(NHC)AuCl] complexes showed that the NHC bonding properties are quite robust against variation of the structure. This study was extended with [(NHC)PPh] adducts and it was shown that the $^{31}$P NMR chemical shift only qualitatively correlates with the $\pi$ acceptor properties of the NHCs.[13] A recent computational study of various [(NHC)AuCl] complexes focused on Au NMR found a correlation between the $\pi$-accepting ability of these complexes and the $^{197}$Au chemical shift.[14] Furthermore, they also found that the paramagnetic shielding tensor of the carbene-C atom is the

[a] Zernike Institute for Advanced Materials, University of Groningen, Nijenborgh 4, 9747 AG, Groningen, The Netherlands
E-mail: maria.a.izquierdo@uv.es
r.w.a.havenith@rug.nl
[b] Institute of Molecular Science, University of Valencia, P.O. Box 22085, 46071 Valencia, Spain
[c] Dipartimento di Chimica, Biologia e Biotecnologie, Università di Perugia, Via Elce di Sotto 8, 06123, Perugia, Italy
[d] Istituto di Scienze e Tecnologie Chimiche del CNR "G. Natta" (SCITEC-CNR), Via Elce di Sotto 8, 06123, Perugia, Italy
[e] Max-Planck-Institut für Kohlenforschung, Kaiser-Wilhelm-Platz 1, 45470, Mülheim an der Ruhr, Germany
[f] Stratingh Institute for Chemistry, University of Groningen, Nijenborgh 4, 9747 AG, Groningen, The Netherlands
[g] Ghent Quantum Chemistry Group, Department of Inorganic and Physical Chemistry, Ghent University, Krijgslaan 281 (S3), B-9000 Gent, Belgium
Supporting information and ORCID(s) from the author(s) for this article are available on the WWW under https://doi.org/10.1002/ejic.201901115.

Full Paper
doi.org/10.1002/ejic.201901115


main shielding term which shows variation by changes in the (NHC) moiety. More NMR studies were performed for [(NHC)-Se] and [(NHC)-P] complexes, and a correlation was established between the Se and P chemical shifts and the ability of the (NHC) ligand to accept π-electron density.[15] No correlation between the $\sigma$-donating contribution and the shielding was found.

NMR spectroscopy, in terms of chemical shifts,[16–19] has been used for understanding the structural and electronic properties of NHCs. The NHC carbon chemical shielding tensor of 1,3,4,5-tetramethylimidazol-2-ylidene (L) is largely anisotropic, as found experimentally by Arduengo et al.[20] That is, the shielding tensor is dominated by a single component, the $\sigma^{yy}$ component (Figure 1) (for a review on the theoretical NMR spectroscopy of NHC, ref.[21]). The anisotropic character of the shielding tensor is preserved in [(NHC)AuL]$^{+/0}$ complexes, as found theoretically by Marchione et al.[22] For a wide range of ligands, the $\sigma^{xx}$ and $\sigma^{zz}$ components remain nearly constant while the $\sigma^{yy}$ component significantly changes. This component lies perpendicular to the (NHC)–Au bond, and largely dominates the isotropic shielding constant, $\sigma$. The bonding and shielding tensor components have been mapped through the Dewar–Chatt–Duncanson (DCD) model[23,24] and the CD-NOCV method.[25] The CD-NOCV method combines the charge displacement (CD) function[26] with the natural orbital chemical valence (NOCV) approach.[27] The NHC→Au $\sigma$-donation component correlates fairly well with the $\sigma^{yy}$ component, and consequently with $\sigma$. However, the reasons why the $\sigma^{yy}$ component dominates over the other components of $\sigma$ are not completely clear yet and only a qualitative picture has been given, mainly based on the Ramsey formula.[28] Questions like which orbitals govern $\sigma$ and what is the influence of L remain unanswered. Clearly, if the anisotropic character is understood, the correlation between the NHC→Au $\sigma$-donation and the $\sigma^{yy}$ component may be rationalized. Thus, an analysis of the shielding tensor given in terms of orbital contributions is highly desirable.

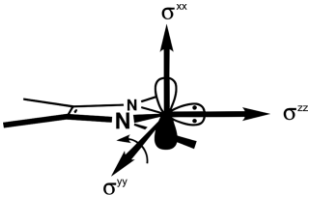


Figure 1. Principal component of the shielding tensor for NHC. The axes orientation identify the orthonormal reference system centered on the NHC carbon, in which the 3 × 3 chemical shielding tensor is diagonal. Image adapted from ref.[20]

Here, a detailed analysis of the shielding tensor in terms of the current density is presented. Among the different current density approaches, the continuous transformation of the current density - diamagnetic zero (CTOCD-*DZ*)[29–34] as implemented in the SYSMO code[35] is used. The advantage of using CTOCD-*DZ* is that it allows a natural decomposition of the shielding tensor into orbital contributions and a spectral analysis.[36] Within CTOCD-*DZ* the first-order current density [$j_n^{(1)}(r)$] is a sum of orbital contributions.

$$j^{(1)}(r) = \sum_{n=1}^{N/2} j_n(r) \quad \text{where } j_n(r) \text{ is:}$$
$$j_n(r) = \frac{ieh}{m}\int(\psi_n \nabla \psi_n^{(1)*} + \psi_n^{(1)*}\nabla\psi_n)dr \qquad (1)$$

and where the first-order correction to the occupied orbital ($\psi_n$), denoted $\psi_n^{(1)}$, is:[31]

$$\psi_n^{(1)} = \frac{e}{2m}\left[d \times \sum_{p>N/2} \psi_p \frac{\langle\psi_p|\hat{p}|\psi_n\rangle}{\epsilon_p - \epsilon_n}\right].B + \frac{e}{2m}\left[d \times \sum_{p>N/2} \psi_p \frac{\langle\psi_p|\hat{l}|\psi_n\rangle}{\epsilon_p - \epsilon_n}\right].B \quad (2)$$

where *N* represents the number of electrons, $\psi_n$ and $\psi_p$ represent the occupied and virtual orbitals, respectively, *B* represents the external magnetic field and *p* and *l* are linear and angular momentum operators, respectively.

By substituting $\psi_n^{(1)}$ in Equation 1, the CTOCD-*DZ* $j_n(r)$ is then expressed in two terms, the conventionally called orbital diamagnetic contribution $j_n^{(d)}(r)$ and the orbital paramagnetic contribution [$j_n^{(p)}(r)$]. The first-order correction $\psi_n^{(1)}$ and therefore also $j_n(r)$ are determined by the accessibility of states through translational transitions [by means of the linear momentum operator ($\hat{p}$)] and rotational transitions [by means of the angular momentum operator $\hat{l}(0)$].[31] A transition $\psi_n \rightarrow \psi_p$ contributes to the induced current and thus the shielding constant if the direct product of $\Gamma(\psi_n) \times \Gamma(\hat{l}) \times \Gamma(\psi_p)$ spans the totally symmetric representation, $\Gamma_0$, of the point group to which the molecule belongs (where $\hat{l}$ represents the operators $\hat{p}$, $\hat{l}$).[31]

## Results and Discussion

A series of complexes with $C_{2v}$ equilibrium geometry having the general formula [(NHC)AuL] or [(NHC)AuL]$^+$ (where NHC stands for imidazol-2-ylidene and L represents the auxiliary ligand) was studied. This series comprises (NHC), [(NHC)H]$^+$, [(NHC)Au]$^+$, [(NHC)AuH], [(NHC)AuCNH]$^+$, [(NHC)AuBr], [(NHC)AuCl], [(NHC)AuCO]$^+$, [(NHC)AuXe]$^+$ and [(NHC)AuPyrrolyl] (Figure 2).

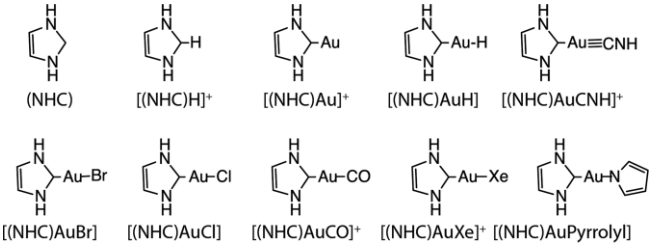


Figure 2. Molecular structures of (NHC), [(NHC)H]$^+$ and [(NHC)AuL]$^{+/0}$ complexes.

These systems represent a suitable subset of those studied in ref.,[22] and as it will be demonstrated, their symmetry properties play a key role in the rationalization of their DCD bonding and the shielding tensor components.

This section begins by briefly summarizing the bond analysis for the systems under study, which has been presented elsewhere.[22] Such analysis is based on the donation and back-donation components of the DCD model and on the electron density rearrangement ($\Delta\rho$) upon formation of [(NHC)AuL]$^{+/0}$, from (NHC) and [AuL]$^{+/0}$. The DCD components are disentangled through the NOCV method, taking as a reference the occupied orbitals of (NHC) and [AuL]$^{+/0}$ suitably orthogonalized to

Full Paper
doi.org/10.1002/ejic.201901115


each other and renormalized (for details, see ref.[25]). $\Delta\rho$ is decomposed into NOCV pairs ($\Delta\rho_k$) which may be easily ascribed to the DCD components, on the basis of their local symmetry. For the systems under study, each NOCV pair belongs to one of the four irreducible representations of the $C_{2v}$ point group ($a_1$, $a_2$, $b_1$ and $b_2$).

The top panel of Figure 3 shows the components of $\Delta\rho$ for [(NHC)AuCl]. $\Delta\rho_1$, the more significant component of $\Delta\rho$, has regions of charge accumulation and depletion on the [AuCl] fragment and the NHC carbon lone-pair, respectively. $\Delta\rho_1$, characterized by a cylindrical symmetry, is ascribed to the $\sigma$-donation component ($\sigma$ don) ($\Delta\rho_k$ with $a_1$ symmetry). $\Delta\rho_2$ and $\Delta\rho_4$ are ascribed to the in-plane and out-of-plane $\pi$-back-donation components ($\Delta\rho_k$ with $b_1$ and $b_2$ symmetries, respectively). The in-plane and out-of-plane $\pi$-back-donation components are denoted in Figure 3 by $\pi_{||}$ and $\pi_{\perp}$, respectively. $\Delta\rho_3$ is ascribed to the $\sigma$-back-donation component ($\sigma$ back), which has been observed in a similar complex, [(S)AuCl] [where S represents 2-(1-hexynyl)dimethylaniline].[37]

Quantitative information of $\Delta\rho$ has been obtained through the CD function. The results are given in Table 1. The data show that L mainly affects the CT$\sigma_{don}$ (CT values range from 0.48 to 0.25 e) and CT$\pi_{\perp}$ (CT values range from 0.00 to –0.12 e) while CT$\pi_{||}$ and CT$\sigma_{back}$ give a systematic small contribution to the CT (whose values range from –0.02 to –0.04 e).

Next, the anisotropic character of the shielding tensor is verified. The results are presented in Table 2. For a given system, the isotropic shielding constant, $\sigma$, is obtained by averaging the three components of the shielding tensor. For completeness, the experimental chemical shift, when available, is also reported.

Calculated and experimental chemical shifts – with a linear regression coefficient, $R^2$, of 0.91- follow the same trend, despite that spin-orbit and solvent effects were not considered in the computations {for a larger series of $[(NHC)AuL]^{+/0}$ complexes, see Table 2 and Figure SI of ref.[22]}. The $\sigma^{yy}$ component varies in a wide range while the $\sigma^{xx}$ and $\sigma^{zz}$ components remain almost constant. The systems are oriented in such a way that the *z* axis is the symmetry axis, the *y* axis lies in the plane of the (NHC) ring and the *x* axis is perpendicular to the *yz* plane (Figure 1). The shielding tensor components are comparable within the series because in all the cases the corresponding component axes coincide. The component orientations are dictated by local $C_{2v}$ symmetry at the (NHC) carbon.

The $\sigma^{yy}$ component originates from the action of the external magnetic field, *B*, in the *y* direction ($B_y$), which induces a current on the *xz* plane. The *xz* plane contains the (NHC) carbon lone pair and its formally empty $p_x$ orbital, participating in the donation and back-donation to and from $[AuL]^{+/0}$, respectively. Thus, $\sigma^{yy}$ is an ideal probe of the electronic properties of $[(NHC)AuL]^{+/0}$.

There is a strong correlation between the $\sigma^{yy}$ and $\sigma$-donation components.[22] There is a less strong correlation between the $\sigma^{yy}$ component and the total CT (CT is a measure of the net acidity of the $[AuL]^{+/0}$ fragment). The correlation is weakened by a significant $\pi_{\perp}$ back-donation, nevertheless, this bonding component does not have a direct effect on the shielding tensor. The reason why only the $\sigma$-donation component modifies the $\sigma^{yy}$ component is not obvious and motivated the following analysis.

Symmetry properties may be used to decompose the isotropic shielding into orbital contributions.[44] Transitions due to the coupling between $\psi_n$ and $\psi_p$ via the operators $\hat{p}$ and $\hat{l}$,

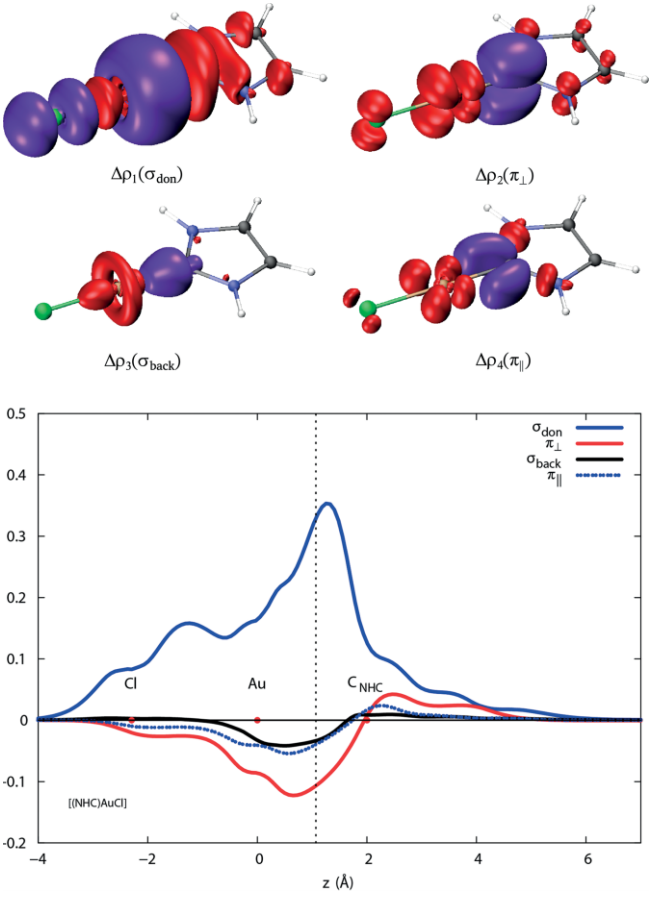


Figure 3. NOCV-CD analysis for [(NHC)AuCl]. Top panel: contribution to deformation density of the four most significant NOCV pairs of [(NHC)AuCl], with [AuCl] and (NHC) fragments. Isodensity surfaces (±0.0015 e/au$^3$) are superimposed to the molecular structure of the complex. Red surfaces (negative values) identify charge depletion regions; purple surfaces (positive values) identify charge accumulation regions. The small green sphere represents the chlorine atom. Bottom panel: CD curves. Red dots indicate the atomic nuclei on the *z* axis, where $C_{NHC}$ represents the (NHC) carbon atom. A dotted vertical line marks the boundary between the [AuCl] and (NHC) fragments in which relative values of CT (CT$\sigma_{don}$, CT$\pi_{\perp}$, CT$\pi_{||}$, CT$\sigma_{back}$) are obtained (for further details, see Computational Details of ref.[22]).

Table 1. CT decomposition into CT$\sigma_{don}$, CT$\pi_{\perp}$, CT$\pi_{||}$, CT$\sigma_{back}$, in e, for $[(NHC)AuL]^{+/0}$.[22]

| System | CT$\sigma_{don}$ | CT$\pi_{\perp}$ | CT$\pi_{||}$ | CT$\sigma_{back}$ | CT |
|---|---|---|---|---|---|
| $[(NHC)Au]^+$ | 0.480 | –0.043 | –0.026 | –0.026 | 0.385 |
| [(NHC)AuH] | 0.246 | –0.075 | –0.032 | –0.019 | 0.120 |
| $[(NHC)AuCNH]^+$ | 0.326 | –0.020 | –0.020 | –0.031 | 0.255 |
| [(NHC)AuBr] | 0.315 | –0.104 | –0.039 | –0.033 | 0.140 |
| [(NHC)AuCl] | 0.313 | –0.107 | –0.040 | –0.040 | 0.126 |
| $[(NHC)AuCO]^+$ | 0.341 | –0.002 | –0.017 | –0.032 | 0.290 |
| $[(NHC)AuXe]^+$ | 0.409 | –0.043 | –0.025 | –0.034 | 0.307 |
| [(NHC)AuPyrrolyl] | 0.302 | –0.118 | –0.035 | – | 0.149 |

Full Paper
doi.org/10.1002/ejic.201901115



Table 2. NHC carbon shielding tensor components and isotropic shielding constant, $\sigma$, of (NHC), $[(NHC)H]^+$ and $[(NHC)AuL]^{+/0}$. Computed values are referenced to (NHC) (chosen as arbitrary zero) as $\Delta\sigma^{ii} = \sigma^{ii}_{NHC} - \sigma^{ii}_{[NHCAuL]+/-}$ and expressed in ppm. $\delta_{exp}$ is the experimental isotropic chemical shift of $[(NHC)^{IPr}AuL]^{+/0}$ relative to TMS; measured in solution where a, b, c and d represent $d_6$-benzene, DMSO, $CDCl_3$ and $CD_2Cl_2$, respectively.

| System | $\Delta\sigma^{xx}$ | $\Delta\sigma^{yy}$ | $\Delta\sigma^{zz}$ | $\Delta\sigma$ | $\delta_{exp}$ |
|---|---|---|---|---|---|
| (NHC) | 0.000 | 0.000 | 0.000 | 0.000 | 220.6[a][38] |
| $[(NHC)H]^+$ | 1.184 | 285.330 | −16.041 | −90.158 | 132.2[b][38] |
| $[(NHC)Au]^+$ | 16.900 | 256.951 | −47.148 | −75.567 | |
| [(NHC)AuH] | 19.098 | 116.545 | −20.950 | −38.231 | 204.9[a][39] |
| $[(NHC)AuCNH]^+$ | 16.770 | 184.368 | −25.193 | −58.648 | 178.3[c][40] |
| [(NHC)AuBr] | 25.074 | 160.993 | −29.120 | −52.315 | 179.0[c][41] |
| [(NHC)AuCl] | 25.610 | 156.694 | −30.612 | −50.564 | 175.5[c][42] |
| $[(NHC)AuCO]^+$ | 16.945 | 193.790 | −25.628 | −61.712 | 174.6[d][43] |
| $[(NHC)AuXe]^+$ | 17.743 | 210.412 | −35.931 | −64.074 | |
| [(NHC)AuPyrrolyl] | 24.182 | 140.876 | −31.171 | −44.629 | |

contribute to $\sigma$.[31] These transitions satisfy the selection rules $\Gamma(\psi_n) \times \Gamma(\hat{l}) \times \Gamma(\psi_p) = \Gamma_0$ with $\hat{l} = \hat{p},\hat{l}$.

Here, $\sigma$ is decomposed into orbital contributions belonging to the $a_1$, $a_2$, $b_1$ and $b_2$ irreducible representations. For each irreducible representation, orbital contributions are grouped, leading to sets of $\psi_n(a_1)$, $\psi_n(a_2)$, $\psi_n(b_1)$ and $\psi_n(b_2)$. The occupied-orbital-symmetry decomposition is presented in Table 3. For a given system, the isotropic shielding constant, $\sigma$, is obtained by adding all the symmetry-contributions.

Table 3 shows that only transitions involving $\psi_n(a_1)$ significantly change, while transitions involving $\psi_n(a_1)$, $\psi_n(b_1)$ and $\psi_n(b_2)$ marginally change. The former correlate with $\sigma$, with a $R^2$ of 0.99 (Figure 4). $\psi_n(b_1)$ and $\psi_n(b_2)$ are related to the $\pi_\perp$ and $\pi_\parallel$ back-donation components, respectively. The fact that $\psi_n(b_1)$ and $\psi_n(b_2)$ do not significantly contribute to the variation of $\sigma$ is consistent with the fact that the $\pi_\parallel$ and $\pi_\perp$ back-donation components have only negligible influence on the chemical shift.

Table 3. Occupied-orbital-symmetry decomposition into $\sigma_k$ components of the (NHC) carbon isotropic shielding constant, $\sigma$, of (NHC), $[(NHC)H]^+$ and $[(NHC)AuL]^{+/0}$ complexes; $\psi_n(a_1)$, $\psi_n(a_2)$, $\psi_n(b_1)$, $\psi_n(b_2)$. All values are expressed in ppm.

| System | $\psi_n(a_1)$ | $\psi_n(a_2)$ | $\psi_n(b_1)$ | $\psi_n(b_2)$ | $\sigma$ |
|---|---|---|---|---|---|
| (NHC) | 29.367 | 2.878 | −24.840 | −63.862 | −56.458 |
| $[(NHC)H]^+$ | 121.986 | 3.399 | −22.882 | −68.803 | 33.700 |
| $[(NHC)Au]^+$ | 115.801 | 4.521 | −23.166 | −78.026 | 19.109 |
| [(NHC)AuH] | 74.776 | 4.160 | −30.173 | −66.991 | −18.227 |
| $[(NHC)AuCNH]^+$ | 95.007 | 4.336 | −28.114 | −69.039 | 2.190 |
| [(NHC)AuBr] | 89.767 | 4.318 | −30.362 | −67.866 | −4.143 |
| [(NHC)AuCl] | 88.055 | 4.324 | −30.587 | −67.687 | −5.894 |
| $[(NHC)AuCO]^+$ | 98.592 | 4.364 | −28.438 | −69.234 | 5.254 |
| $[(NHC)AuXe]^+$ | 103.262 | 4.425 | −26.626 | −73.444 | 7.616 |
| [(NHC)AuPyrrolyl] | 82.341 | 4.201 | −31.310 | −67.061 | −11.829 |

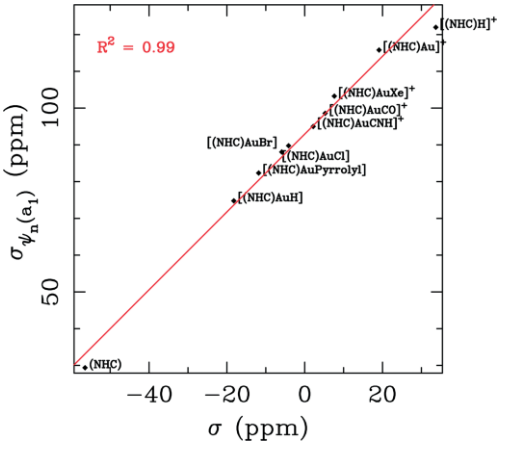


Figure 4. Correlation between the $\psi_n(a_1)$ component and the isotropic shielding constant, $\sigma$, of the (NHC) carbon atom for (NHC), $[(NHC)H]^+$ and $[(NHC)AuL]^{+/0}$ complexes.

A further orbital partitioning into translational and rotational contributions is reported in Table 4 (Equation 2); for completeness translational and rotational contributions involving $\psi_n(a_2)$, $\psi_n(b_1)$ and $\psi_n(b_2)$ are also reported. For a given system, the isotropic shielding constant, $\sigma$, is obtained by adding all the translational and rotational contributions.

Table 4 shows only a very weak correlation of the $\sigma^{rot}_{\psi_n(a_1)}B_j$ component with the isotropic shielding, with a $R^2$ of 0.76 (see also Figure 5).

The rotational contributions may be further decomposed, restricting the lay axis of $B$ to the $y$ direction. The results are given in Table 5, where $\sigma^{rot,yy}_{\psi_n(a_1)}B_y$ represents the $\sigma^{yy}$ component of rotational transitions, $\langle\psi_n(a_1)|\hat{l}_y(b_1)|\psi_p(b_1)\rangle$, under the action of the external magnetic field $B$ along the $y$ axis. For completeness $\sigma^{rot,xx}_{\psi_n(a_1)}B_x$ and $\sigma^{rot,zz}_{\psi_n(a_1)}B_z$ contributions are also reported. For a given system, the orbital-orbital rotational contribution, reported in

Table 4. Occupied-orbital-symmetry decomposition into $\sigma_k^{i,j}B_{xyz}$ components of the (NHC) carbon isotropic shielding constant, $\sigma$, of (NHC), $[(NHC)H]^+$ and $[(NHC)AuL]^{+/0}$ complexes; $i,j$ = *trans,rot* and $k = \psi_n(a_1)$, $\psi_n(a_2)$, $\psi_n(b_1)$, $\psi_n(b_2)$ (for simplicity $B_{xyz}$ is omitted). $R^2$ is the linear regression coefficient between each component and $\sigma$. All values are expressed in ppm.

| System | $\sigma^{trans}_{\psi_n(a_1)}B_j$ | $\sigma^{rot}_{\psi_n(a_1)}B_j$ | $\sigma^{rot}_{\psi_n(a_2)}B_j$ | $\sigma^{rot}_{\psi_n(a_2)}B_j$ | $\sigma^{trans}_{\psi_n(b_1)}B_j$ | $\sigma^{rot}_{\psi_n(b_1)}B_j$ | $\sigma^{trans}_{\psi_n(b_2)}B_j$ | $\sigma^{rot}_{\psi_n(b_2)}B_j$ | $\sigma$ |
|---|---|---|---|---|---|---|---|---|---|
| (NHC) | 301.371 | −272.009 | 8.923 | −6.046 | 23.515 | −48.354 | −7.451 | −56.409 | −56.458 |
| $[(NHC)H]^+$ | 317.754 | −195.768 | 10.456 | −7.058 | 23.592 | −46.474 | −2.669 | −66.135 | 33.700 |
| $[(NHC)Au]^+$ | 330.956 | −215.154 | 36.082 | −31.561 | 52.681 | −75.868 | 70.385 | −148.411 | 19.109 |
| [(NHC)AuH] | 316.692 | −241.000 | 34.935 | −30.774 | 47.947 | −78.120 | 111.694 | −178.686 | −18.227 |
| $[(NHC)AuCNH]^+$ | 295.939 | −201.049 | 36.237 | −31.901 | 49.510 | −77.624 | 175.887 | −244.926 | 2.190 |
| [(NHC)AuBr] | 322.906 | −233.136 | 37.280 | −32.961 | 60.461 | −90.823 | 142.460 | −210.327 | −4.143 |
| [(NHC)AuCl] | 314.567 | −226.512 | 35.459 | −31.135 | 55.774 | −86.362 | 142.288 | −209.975 | −5.894 |
| $[(NHC)AuCO]^+$ | 309.706 | −211.115 | 36.069 | −31.705 | 51.188 | −79.627 | 150.729 | −219.963 | 5.254 |
| $[(NHC)AuXe]^+$ | 318.783 | −215.388 | 39.396 | −34.970 | 48.172 | −74.799 | 146.397 | −219.841 | 7.616 |
| [(NHC)AuPyrrolyl] | 289.687 | −207.435 | 39.435 | −35.234 | 48.279 | −79.589 | 212.977 | −280.039 | −11.829 |
| $R^2$ | 0.21 | 0.76 | 0.05 | 0.04 | 0.04 | 0.01 | 0.01 | 0.01 | |

Full Paper
doi.org/10.1002/ejic.201901115



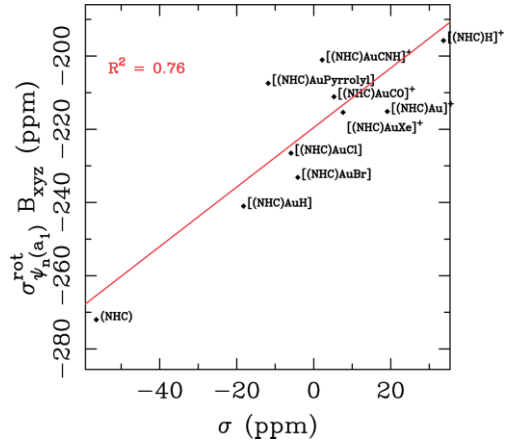


Figure 5. Correlation between the $\sigma^{rot}_{\psi_n(a_1)}B_jB_{xyz}$ component and the isotropic shielding constant, $\sigma$, of the (NHC) carbon atom for (NHC), $[(NHC)H]^+$ and $[(NHC)AuL]^{+/0}$ complexes.

Table 4, is obtained by averaging all the contributions [$\sigma^{rot,xx}_{\psi_n(a_1)}B_x$ and $\sigma^{rot,xx}_{\psi_n(a_1)}B_x$ represent the $\langle\psi_n(a_1)|\hat{l}_x(b_2)|\psi_p(b_2)\rangle$ and $\langle\psi_n(a_1)|\hat{l}_z(a_2)|\psi_p(a_2)\rangle$ transitions, respectively]. Note that each $\sigma^{rot,yy}_{\psi_n(a_1)}B_y$ contribution reported in Table 5 includes grouped $\psi_n(a_1)\rightarrow\psi_p(b_1)$ transitions. For instance, (NHC) and $[(NHC)H]^+$ have 9 $\psi_n(a_1)$, $[(NHC)Au]^+$ has 13 $\psi_n(a_1)$, [(NHC)AuCl] and $[(NHC)AuCO]^+$ have 18 $\psi_n(a_1)$ and so on.

Table 5. Decomposition of the $\sigma^{rot}_{\psi_n(a_1)}B_jB_{xyz}$ component into $\sigma^{rot,i}_{\psi_n(a_1)}B_j$ contributions of the (NHC) carbon for (NHC), $[(NHC)H]^+$ and $[(NHC)AuL]^{+/0}$ complexes; *i* = *xx*, *yy*, *zz*; *j* = *x*, *y*, *z*. All values are expressed in ppm.

| System | $\sigma^{rot,xx}_{\psi_n(a_1)}B_x$ | $\sigma^{rot,yy}_{\psi_n(a_1)}B_y$ | $\sigma^{rot,zz}_{\psi_n(a_1)}B_z$ | $\sigma^{rot}_{\psi_n(a_1)}B_jB_{xyz}$ |
|---|---|---|---|---|
| (NHC) | −34.815 | −493.434 | −287.778 | −272.009 |
| $[(NHC)H]^+$ | −37.163 | −248.160 | −300.292 | −195.768 |
| $[(NHC)Au]^+$ | −36.277 | −334.339 | −274.535 | −215.154 |
| [(NHC)AuH] | −35.356 | −473.243 | −217.348 | −241.000 |
| $[(NHC)AuCNH]^+$ | −35.839 | −444.944 | −122.448 | −201.049 |
| [(NHC)AuBr] | −35.428 | −455.745 | −208.234 | −233.136 |
| [(NHC)AuCl] | −35.366 | −451.421 | −192.749 | −226.512 |
| $[(NHC)AuCO]^+$ | −36.070 | −428.864 | −168.109 | −211.115 |
| $[(NHC)AuXe]^+$ | −72.197 | −383.149 | −190.684 | −215.388 |
| [(NHC)AuPyrrolyl] | −37.368 | −502.401 | −94.498 | −207.435 |

As observed in Table 5, the $\sigma^{rot,yy}_{\psi_n(a_1)}B_y$ contribution varies considerably. When excluding (NHC), $\sigma^{rot,yy}_{\psi_n(a_1)}B_y$ and $\sigma$ fairly correlate, with a $R^2$ of 0.92 (Figure 6). The linear regression coefficients for $\sigma^{rot,zz}_{\psi_n(a_1)}B_z$ and $\sigma^{rot,zz}_{\psi_n(a_1)}B_z$ with $\sigma$ are 0.02 and 0.42, respectively. This clearly shows that rotational transitions of the type $\psi_n(a_1)\rightarrow\psi_p(b_1)$ dominate the variation of $\sigma$.

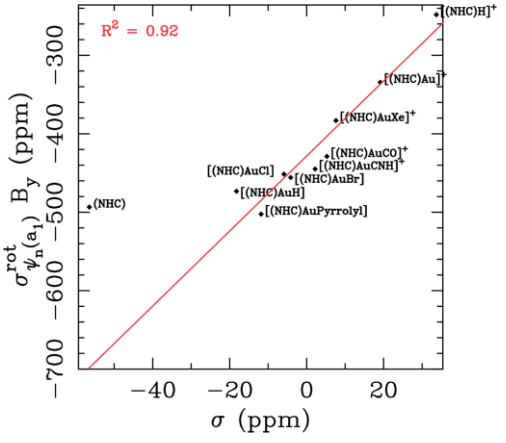


Figure 6. Correlation between the $\sigma^{rot,yy}_{\psi_n(a_1)}B_y$ component and the isotropic shielding constant, $\sigma$, of the (NHC) carbon atom for (NHC), $[(NHC)H]^+$ and $[(NHC)AuL]^{+/0}$ complexes.

Each $\sigma^{rot,yy}_{\psi_n(a_1)}B_y$ contribution depends on the matrix elements $[\langle\psi_n(a_1)|\hat{l}_y(b_1)|\psi_p(b_1)\rangle]$ and on the reciprocal of the energy difference between the occupied and virtual orbitals ($\in_p - \in_n$). Ideally, the dominant transitions should be recognizable. However, for the systems under study several transitions contribute to $\sigma^{rot,yy}_{\psi_n(a_1)}B_y$. For instance, selecting the $\psi_n(a_1)\rightarrow\psi_p(b_1)$ transitions which ratio between $\langle\psi_n(a_1)|\hat{l}_y(b_1)|\psi_p(b_1)\rangle$ and its corresponding $\in_p - \in_n$ is greater than 1 (Equation 2), would include at most four transitions, as seen in Table 6. However, for some systems,

Table 6. Largest $\sigma^{rot,yy}_{\psi_n(a_1)}B_y$ contributions to the $\sigma^{yy}$ tensor component of (NHC), $[(NHC)H]^+$ and $[(NHC)AuL]^{+/0}$ in ppm, and their $\in_{b_1} - \in_{a_1}$, in eV. 'Quota' stands for the ratio between $\langle\psi_n(a_1)|\hat{l}_y(b_1)|\psi_p(b_1)\rangle$ and its corresponding $\in_p - \in_n$, $\Delta\sigma^{rot,yy}_{\psi_n(a_1)}B_y$ stands for the difference between all $\sigma^{rot,yy}_{\psi_n(a_1)}B_y$ transitions and selected $\psi_n(a_1)\rightarrow\psi_p(b_1)$ $\sigma^{rot,yy}_{\psi_n(a_1)}B_y$ transitions. $\in_{b_1}$.

| System | $\psi_n(a_1)\rightarrow\psi_p(b_1)$ | Quota | $\in_{a_1}$ | $\in_{b_1}$ | $\in_{b_1} - \in_{a_1}$ | $\psi_n(a_1)\rightarrow\psi_p(b_1)$ $\sigma^{rot,yy}_{\psi_n(a_1)}B_y$ | $\Delta\sigma^{rot,yy}_{\psi_n(a_1)}B_y$ |
|---|---|---|---|---|---|---|---|
| (NHC) | 18 → 21 | 6.092 | −4.818 | 0.039 | 4.779 | −642.744 | 149.309 |
| $[(NHC)H]^+$ | 14 → 19 | 3.579 | −16.837 | −6.777 | 10.060 | −289.038 | 40.858 |
| $[(NHC)Au]^+$ | 20 → 29 | 3.071 | −15.463 | −6.231 | 9.232 | −212.058 | −34.290 |
| | 26 → 29 | 2.953 | −11.313 | −6.231 | 5.082 | −88.033 | |
| [(NHC)AuH] | 20→ 29 | 3.373 | −9.901 | −1.319 | 8.582 | −233.162 | −240.081 |
| $[(NHC)AuCNH]^+$ | 20 → 37 | 2.106 | −16.526 | −4.701 | 11.825 | −50.207 | −233.784 |
| | 27 → 37 | 2.098 | −12.790 | −4.701 | 8.089 | −160.953 | |
| [(NHC)AuBr] | 35 → 46 | 3.444 | −10.558 | −1.712 | 8.846 | −268.718 | −187.027 |
| [(NHC)AuCl] | 26 → 37 | 3.371 | −10.623 | −1.675 | 8.948 | −257.891 | −193.53 |
| $[(NHC)AuCO]^+$ | 21 → 37 | 2.827 | −16.893 | −5.353 | 11.540 | −58.638 | −115.277 |
| | 27 → 37 | 2.223 | −13.553 | −5.353 | 8.200 | −174.919 | |
| | 27 → 42 | 1.930 | −13.553 | −3.547 | 10.006 | −83.336 | |
| $[(NHC)AuXe]^+$ | 29 → 42 | 3.050 | −15.124 | −5.628 | 9.496 | −139.337 | −69.361 |
| | 31 → 46 | 3.840 | −12.956 | −3.732 | 9.224 | −154.450 | |
| [(NHC)AuPyrrolyl] | 26 → 46 | 1.953 | −12.122 | −1.674 | 10.448 | −41.721 | −300.470 |
| | 31 → 46 | 1.133 | −10.194 | −1.674 | 8.520 | −75.243 | |
| | 31 → 52 | 1.254 | −10.194 | 0.089 | 10.105 | −47.015 | |
| | 31 → 56 | 2.807 | −10.194 | 1.265 | 11.459 | −37.950 | |

Full Paper
doi.org/10.1002/ejic.201901115


this would leave out other non-negligible transitions. For neutral complexes, selected $\psi_n(a_1)\rightarrow\psi_p(b_1)$ $\sigma^{rot,yy}_{\psi_n(a_1)}B_y$ transitions lead to around 50 % of the $\sigma^{rot,yy}_{\psi_n(a_1)}B_y$ contribution. For charged complexes, [(NHC)AuCO]$^+$, [(NHC)AuXe]$^+$ and [(NHC)Au]$^+$ selected $\psi_n(a_1)\rightarrow\psi_p(b_1)$ $\sigma^{rot,yy}_{\psi_n(a_1)}B_y$ transitions cover a larger portion of the $\sigma^{rot,yy}_{\psi_n(a_1)}B_y$ contribution, about 75 %. In contrast, for [(NHC)AuCNH]$^+$, selected $\psi_n(a_1)\rightarrow\psi_p(b_1)$ $\sigma^{rot,yy}_{\psi_n(a_1)}B_y$ transitions cover 47 % of the $\sigma^{rot,yy}_{\psi_n(a_1)}B_y$ contribution.

$\psi_n(a_1)$ and $\psi_n(b_1)$ involved in the $\sigma^{rot,yy}_{\psi_n(a_1)}B_y$ transitions are significantly delocalized, thus, a correlation between the electronic structure of the systems and the NMR parameters is not straightforward (Figure 7). The analysis of $\langle\psi_n(a_1)|\hat{l}_y(b_1)|\psi_p(b_1)\rangle$ may provide insights in this regard. The effect of the angular momentum operator $\hat{l}_y$ appears as a simple 90 degrees rotation of the orbital along the principal *y* axis.[44] There is a significant contribution to $\sigma$ only if the rotated orbital $\hat{l}_y(b_1)\psi_p(b_1)$ overlaps with an occupied orbital ($\psi_n(a_1)|$). Figure 7 shows for (NHC), [(NHC)Au]$^+$ and [(NHC)AuCl] the contour plots of $\psi_n(a_1)$ and $\psi_n(b_1)$ that give the most significant contribution to $\sigma^{rot,yy}_{\psi_n(a_1)}B_y$. It is eye-catching that across the systems $\psi_n(a_1)$ and $\psi_n(b_1)$ are very similar, particularly around the (NHC) carbon atom. The $p_x$ character of the $\psi_n(b_1)$, being largely dominated by the electronic structure of (NHC), is expected to be preserved across the series. The $p_z$ character of $\psi_n(a_1)$ is influenced by the $\sigma$-acidity of the metal fragment. Note that for the selected transitions, $\in_p - \in_n$ does not vary significantly. This suggests that the induced current density is mainly governed by the transition matrix elements rather than the orbital energy difference.

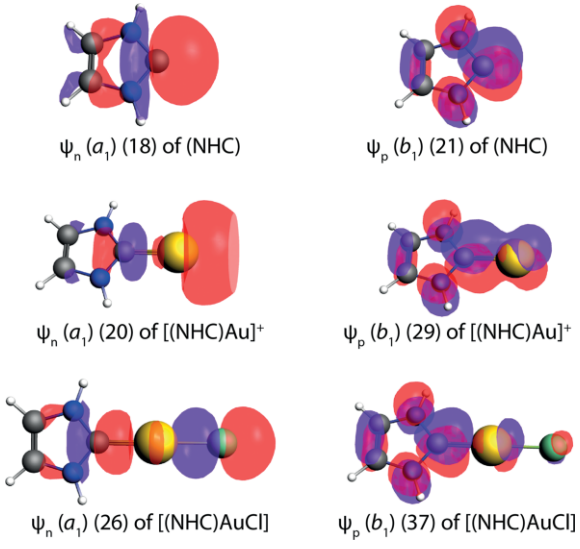


Figure 7. Contour plots of $\psi_n(a_1)$ and $\psi_n(b_1)$ involved in the dominant $\psi_n(a_1)\rightarrow\psi_p(b_1)$ transition of (NHC), [(NHC)Au]$^+$ and [(NHC)AuCl] complexes. Isodensity surfaces (±0.003 e/au$^3$) are superimposed to the molecular structure of the complex.

## Conclusions

In the framework of the CTOCD-*DZ* formulation, the shielding tensor of the (NHC) carbon atom in [(NHC)AuL]$^{+/0}$ complexes was systematically analyzed. Emphasis was given to the anisotropic character of the shielding tensor, considering that only one of its three components, $\sigma^{yy}$, significantly varies along the series. Progressive decomposition of the chemical shielding tensor into orbital contributions and a spectral decomposition revealed that its anisotropic character is governed by $\psi_n(a_1)\rightarrow\psi_p(b_1)$ rotational transitions. Along the series, not a single $\psi_n(a_1)\rightarrow\psi_p(b_1)$ rotational transition but a few transitions dominate the isotropic shielding. These transitions, so-called $\sigma^{rot,yy}_{\psi_n(a_1)}B_y$ transitions, occur between occupied and virtual orbitals with strong $p_z(a_1)$ and $p_x(b_1)$ characters (symmetries), respectively. The $\sigma$-donation component, associated to $\psi_n(a_1)$, correlates with the isotropic shielding. The $\pi_{\parallel}$ and $\pi_{\perp}$ back-donation components associated to $\psi_n(b_1)$ and $\psi_n(b_2)$, respectively, have a negligible influence on the chemical shift because rotational transitions from $\psi_n(b_1)$ and $\psi_n(b_2)$ do not significantly contribute to the variation of the isotropic shielding. The carbon chemical shielding of [(NHC)AuL]$^{+/0}$ is mainly governed by the transition matrix elements rather than by the orbital energy difference, since the latter remains fairly constant. The presented orbital decomposition analysis contributes to clarify the relationship between the isotropic shielding and the nature of the [(NHC)–AuL]$^{+/0}$ bond, thus, it may be used for quantifying other magnetic properties for [(NHC)-Au] based complexes or different substrate-metal fragments.

## Computational Methods

Geometry optimizations and electron densities of all structures were calculated using density functional theory (DFT). Specifically, the BLYP exchange correlation functional[45,46] in combination with the TZ2P basis set were used. Scalar and spin-orbit relativistic effects were included via the zeroth-order regular approximation (ZORA) as implemented in ADF.[47–50] The NMR constants were computed using the CTOCD-*DZ* formulation,[31] as implemented in the SYSMO code.[35] An intermediate step between the optimized geometry and the actual calculation of the magnetic properties was needed. Starting from optimized structures, the perturbed Kohn–Sham orbitals[31,51,52] were calculated, using GAMESS-UK,[53] with the BLYP exchange correlation functional[45,46] and the uncontracted (u) cc-pV5Z basis set (for the basis set calibration, moving from Slater type orbitals within ADF to Gaussian type orbitals within GAMESS-UK, see Supporting Information). For the calculations with GAMESS-UK the scalar relativistic effects were included via effective core potentials, by using the energy-adjusted pseudo potential developed by Figgen et al.[54]

## *Acknowledgments*

This work was part of a European Joint Doctorate (EJD) in Theoretical Chemistry and Computational Modelling (TCCM), which was financed under the framework of the Innovative Training Networks (ITN) of the MARIE Skłodowska-CURIE Actions (ITN-EJD-642294-TCCM).

**Keywords:** Carbene ligands · Gold · Chemical shielding tensor · Electron donation · Electron back-donation

[1] D. Enders, O. Niemeier, A. Henseler, *Chem. Rev.* **2007**, *107*, 5606–5655.
[2] W. A. Hermann, C. Koecher, *Angew. Chem. Int. Ed.* **1997**, *36*, 2161–2187; *Angew. Chem.* **1997**, *109*, 2256–2282 .

[3] D. Bourissou, O. Guerret, F. P. Gabbai, G. Bertrand, *Chem. Rev.* **2000**, *100*, 39–92.
[4] G. Ung, G. Bertrand, *Angew. Chem. Int. Ed.* **2013**, *52*, 11388–11391; *Angew. Chem.* **2013**, *125*, 11599–11602.
[5] N. Salvi, L. Belpassi, F. Tarantelli, *Chem. Eur. J.* **2010**, *16*, 7231–7240.
[6] A. Comas-Vives, J. Harvey, *Eur. J. Inorg. Chem.* **2011**, *2011*, 5025–5035.
[7] D. J. Nelson, S. P. Nolan, *Chem. Soc. Rev.* **2013**, *42*, 6723–6753.
[8] D. Marchione, L. Belpassi, G. Bistoni, A. Macchioni, F. Tarantelli, D. Zuccaccia, *Organometallics* **2014**, *33*, 4200–4208.
[9] M. N. Hopkinson, C. Richter, M. Schedler, F. Glorius, *Nature* **2014**, *510*, 485–496.
[10] V. H. L. Wong, A. J. P. White, T. S. Andy Hor, K. K. Hii, *Chem. Commun.* **2015**, *51*, 17752–17755.
[11] D. Nemcsok, K. Wichmann, G. Frenking, *Organometallics* **2004**, *23*, 3640–3646.
[12] J. Nitsch, L. P. Wolters, C. Fonseca Guerra, F. M. Bickelhaupt, A. Steffen, *Chem. Eur. J.* **2017**, *23*, 614–622.
[13] C. A. Gaggioli, G. Bistoni, G. Ciancaleoni, F. Tarantelli, L. Belpassi, P. Belanzoni, *Chem. Eur. J.* **2017**, *23*, 7558–7569.
[14] L. M. Azofra, R. M. P. Veenboer, L. Falivene, S. V. C. Vummaleti, A. Poater, S. P. Nolan, L. Cavallo, *Phys. Chem. Chem. Phys.* **2019**, *21*, 15615–15622.
[15] S. V. C. Vummaleti, D. J. Nelson, A. Poater, A. Gómez-Suárez, D. B. Cordes, A. M. Z. Slawin, S. P. Nolan, L. Cavallo, *Chem. Sci.* **2015**, *6*, 1895–1904.
[16] K. W. Zilm, R. A. Merril, M. M. Greenberg, J. A. Berson, *J. Am. Chem. Soc.* **1987**, *109*, 1567–1569.
[17] M. M. Greenberg, S. C. Blackstock, J. A. Berson, R. A. Merril, J. C. Duchamp, K. W. Zilm, *J. Am. Chem. Soc.* **1991**, *113*, 2318–2319.
[18] C. P. Gordon, C. Raynaud, R. A. Andersen, C. Copéret, O. Eisenstein, *Acc. Chem. Res.* **2019**, *52*, 2278–2289.
[19] K. W. Zilm, R. A. Merril, G. G. Webb, M. M. Greenberg, J. A. Berson, *J. Am. Chem. Soc.* **1989**, *111*, 1533–1535.
[20] A. J. Arduengo III, D. A. Dixon, K. K. Kumashiro, C. Lee, W. P. Powder, K. W. Zilm, *J. Am. Chem. Soc.* **1994**, *116*, 6361–6367.
[21] L. Falivene, L. Cavallo, *Coord. Chem. Rev.* **2017**, *344*, 101–114.
[22] D. Marchione, M. A. Izquierdo, G. Bistoni, R. W. A. Havenith, A. Macchioni, D. Zuccaccia, F. Tarantelli, L. Belpassi, *Chem. Eur. J.* **2017**, *23*, 2722–2728.
[23] J. Dewar, *Bol. Soc. Quim. Peru* **1951**, *18*, C71–C79.
[24] J. Chatt, L. A. Duncanson, *J. Chem. Soc.* **1953**, 2939–2947.
[25] G. Bistoni, L. Belpassi, F. Tarantelli, *J. Chem. Phys.* **2015**, *142*, 084112.
[26] L. Belpassi, I. Infante, F. Tarantelli, L. Visscher, *J. Am. Chem. Soc.* **2008**, *130*, 1048–1060.
[27] J. Mrozek, R. F. Nalewajski, A. Michalak, *Pol. J. Chem.* **1998**, *72*, 1779–1791.
[28] N. F. Ramsey, *Phys. Rev.* **1950**, *78*, 699–703.
[29] E. Steiner, P. W. Fowler, *J. Phys. Chem. A* **2001**, *105*, 9553–9562.
[30] R. W. A. Havenith, F. de Proft, P. W. Fowler, P. Geerlings, *Chem. Phys. Lett.* **2005**, *407*, 391–396.
[31] E. Steiner, P. W. Fowler, *Phys. Chem. Chem. Phys.* **2004**, *6*, 261–272.
[32] S. Coriani, P. Lazzeretti, M. Malagoli, R. Zanasi, *Theor. Chim. Acta* **1994**, *89*, 181–192.
[33] T. Keith, R. F. W. Bader, *Chem. Phys. Lett.* **1993**, *210*, 223–231.
[34] P. Lazzeretti, M. Malagoli, R. Zanasi, *Chem. Phys. Lett.* **1994**, *220*, 299–304.
[35] P. Lazzeretti, R. Zanasi, *SYSMO Package, University of Modena*, **1980**. Additional routines by P. W. Fowler, E. Steiner, R. W. A. Havenith, A. Soncini.
[36] E. Steiner, A. Soncini, P. W. Fowler, *J. Phys. Chem. A* **2006**, *110*, 12882–12886.
[37] L. Biasiolo, L. Belpassi, C. A. Gaggioli, A. Macchioni, F. Tarantelli, G. Ciancaleoni, D. Zuccaccia, *Organometallics* **2016**, *35*, 595–604.
[38] D. Tapu, D. A. Dixon, C. Roe, *Chem. Rev.* **2009**, *109*, 3385–3407.
[39] E. Y. Tsui, P. M_ller, J. P. Sadighi, *Angew. Chem. Int. Ed.* **2008**, *47*, 8937–8940; *Angew. Chem.* **2008**, *120*, 9069–9072.
[40] L. Canovese, F. Visentin, C. Levi, V. Bertolasi, *Organometallics* **2011**, *30*, 875–883.
[41] P. de Fremont, R. Singh, E. D. Stevens, J. L. Petersen, S. P. Nolan, *Organometallics* **2007**, *26*, 1376–1385.
[42] S. Gaillard, P. Nun, A. M. Z. Slawin, S. P. Nolan, *Organometallics* **2010**, *29*, 5402–5408.
[43] C. Dash, P. Kroll, M. Yousufuddin, H. V. R. Dias, *Chem. Commun.* **2011**, *47*, 4478–4480.
[44] C. M. Widdifield, R. W. Schurko, *Concepts Magn. Reson. Part A* **2009**, *34*, 91–123.
[45] A. D. Becke, *Phys. Rev. A* **1988**, *38*, 3098–3100.
[46] C. Lee, W. Yang, R. G. Parr, *Phys. Rev. B* **1988**, *37*, 785–789.
[47] G. te Velde, F. M. Bickelhaupt, E. J. Baerends, C. Fonseca-Guerra, S. J. A. van Gisbergen, J. G. Snijders, T. Ziegler, *J. Comput. Chem.* **2001**, *22*, 931–967.
[48] E. van Lenthe, E. J. Baerends, J. G. Snijders, *J. Chem. Phys.* **1993**, *99*, 4597–4610.
[49] E. van Lenthe, E. J. Baerends, J. G. Snijders, *J. Chem. Phys.* **1994**, *101*, 9783–9792.
[50] E. van Lenthe, A. Ehlers, E. J. Baerends, *J. Chem. Phys.* **1999**, *110*, 8943–8953.
[51] E. Steiner, P. W. Fowler, R. W. A. Havenith, *J. Phys. Chem. A* **2002**, *106*, 7048–7056.
[52] R. W. A. Havenith, P. W. Fowler, *Chem. Phys. Lett.* **2007**, *449*, 347–353.
[53] M. F. Guest, I. J. Bush, H. J. J. van Dam, P. Sherwood, J. M. H. Thomas, J. H. van Lenthe, R. W. A. Havenith, J. Kendrick, *Mol. Phys.* **2005**, *103*, 719–747.
[54] D. Figgen, G. Rauhut, M. Dolg, H. Stoll, *Chem. Phys.* **2005**, *311*, 227–244.

Received: October 17, 2019